A Novel Digital Circuit for Position Sensor De-modulation Using Advanced FPGA, Including Field Experience with a 1.45MW Motor Driven Compressor.

Richard Jayawant[1] and Steve Dabbs[1]
[1]Waukesha Magnetic Bearings, Worthing, U.K.
rjayawant@waukbearing.com, sdabbs@waukbearing.com

Abstract

This paper describes a novel demodulation circuit which has been developed for use with inductive position sensors for Active Magnetic Bearing applications. The circuit is designed to operate with conventional bridge type inductive position sensors. This circuit is novel in that the implementation is fully digital and uses a mixture of FPGA and DSP to ensure noise immune phase sensitive de-modulation.

We present the architecture and implementation of the new circuit. The techniques to perform the phase sensitive de-modulation are described, including the techniques necessary to handle the phase shifts due to cable capacitance. In conventional analogue based systems these phase shifts are compensated by field changes to component values.

The experience of using this sensor on a 1.5MW motor driven hydrogen compressor is described. We present the results and experiences of commissioning the machine. The noise levels recorded during testing, and the overall response of the machine both whilst levitated (non-rotating) and during operation are included.

We finish with a comparison of the two methodologies; the precision analogue circuitry versus the digital along with our conclusions.

1 Introduction

Bridge type inductive position sensors used for magnetic bearing applications (as shown in Figure 1) have traditionally used a phase sensitive de-modulation circuit implemented using analogue electronics. In order to optimize the performance of the phase sensitive de-modulation circuit, the phase of the reference waveform should be adjusted to match the phase of the output signal from the sensor (with the rotor displaced from the centre position). With the analogue de-modulation circuits, this phase shifting has been performed using RC filter networks which are matched when the system is in its final installation with the field cabling installed.

A number of references are available which describe the principals and construction of such sensors, including (Traxler & Maslen, 2009). For a comprehensive review of the synchronous de-modulation techniques (also referred to as lock in amplifiers), refer to (Burdett, 2005).

With the move towards automated and remote commissioning of magnetic bearing systems, this type of adjustment within the controller circuitry is inconvenient and a method of optimizing the phase of the demodulation circuit remotely or automatically is desirable. Digitally controlled analogue elements could be used, but a fully digital sensor circuit provides a less complex solution.

Techniques for digital demodulation of such signals have been explored by others: Rahal et al. (Rahal & Demosthenous, 2009) describe an ASIC (Application Specific Integrated Circuit) implementation of such signal conditioning, but this uses demodulation in the analogue domain and consequently the phase is not readily tuned. Dam et al. (Dam, Banerjee, Majumdar, Banerjee, & Patranabis, 2005) describe an FPGA (Fuse Programmable Gate Array) implementation of a phase sensitive de-modulation circuit which uses four samples per cycle together with a priori information regarding the sensor phase delay at the carrier frequency to construct in phase and quadrature magnitude values. While this scheme is able to cope with the phase reversal due to modulation around the sensor null position, it is not clear how well this scheme will handle variable phase shifts due to mismatched impedances in the sensor bridge elements, which will occur in practice and /or variations in the amplitude of the sensor drive signal. While the preceding article used four samples per cycle to determine the peak in phase amplitude, Wu and Hong (Wu & Hong, 2010) looked at the impact of the number of samples per cycle on the accuracy of amplitude measurement. In particular they looked at the accuracy of using five samples per cycle.

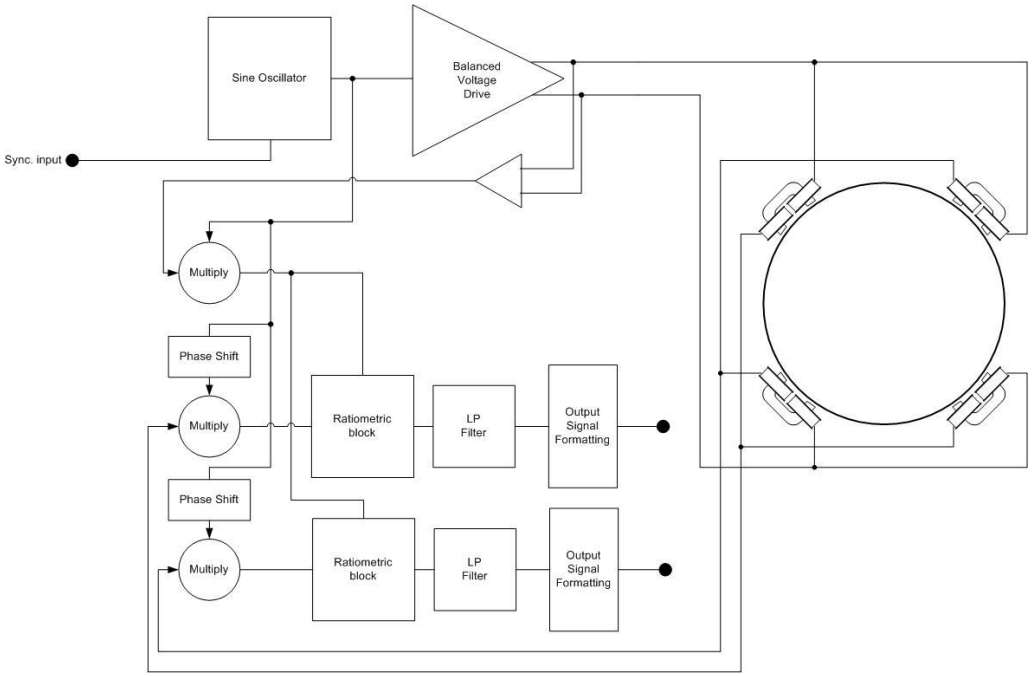

Figure 1- Conventional Inductive Sensor Structure

2 The Novel Sensor Circuit

The novel sensor circuit is integrated within the Waukesha Zephyr magnetic bearing controller. The structure of the circuit combines FPGAs to handle the phase shifting and multiplication functions and DSPs (Digital Signal Processors) to handle the ratio-metric function (in addition to normal magnetic bearing servo control functions).

The architecture of the circuit is shown in Figure 2. A programmable signal generator is used to construct the sine wave at the required carrier frequency. This drive signal is amplified and transmitted as a balanced drive to the sensors. In addition to the sine wave, the generator outputs a synchronizing pulse. The signal generator is under the control of a supervisory FPGA (drive FPGA) which is also responsible for data communications and the supervisory state machine that controls the sequencing of the overall control system. In addition to the sine wave, the signal generator outputs a synchronizing pulse to the drive FPGA.

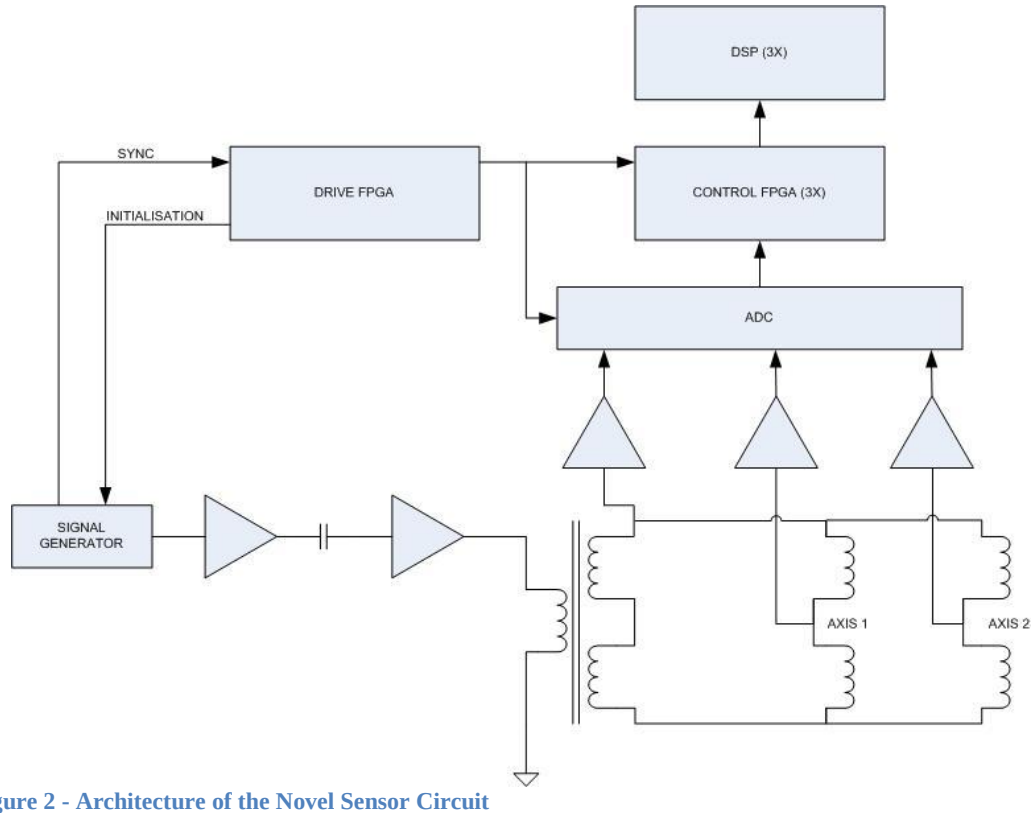

Figure 2 - Architecture of the Novel Sensor Circuit

Each bearing (3 in total) has its own FPGA (control FPGA) and DSP. The synchronization pulses from the drive FPGA are transmitted to each control FPGA and control the timing of the sampling. The drive waveform is sampled together with the waveforms for the returned sensor signals.

The hardware is implemented on a single control card which also handles the servo control, supervisory control and data communications functions of the AMB controller. The control card is shown in Figure 3.

The sampling occurs at 8 times the carrier frequency of the sensor drive. This allows 8 data points per cycle (for each waveform) to be captured by the FPGA and used in the computations. In addition to the sampled data, there is a look up table within the FPGA which has the nominal value for a unity amplitude Sine wave. This look up table contains 32 values per cycle.

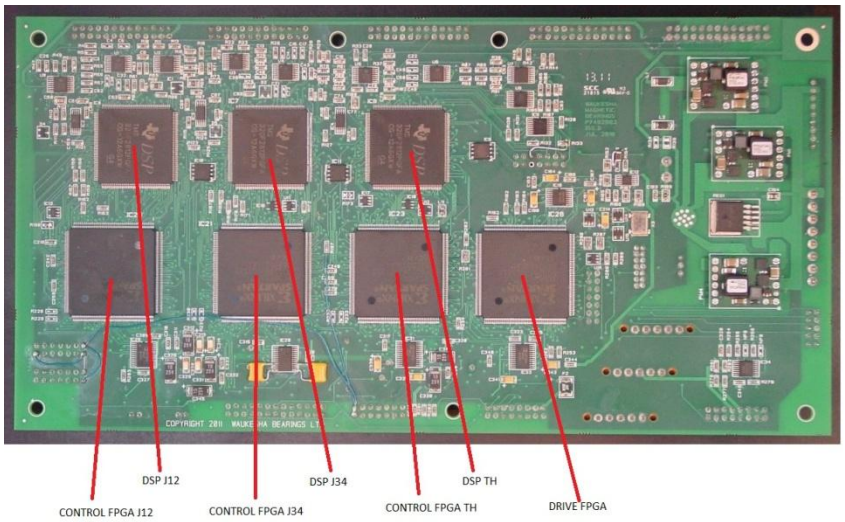

Figure 3 - Control Card Hardware

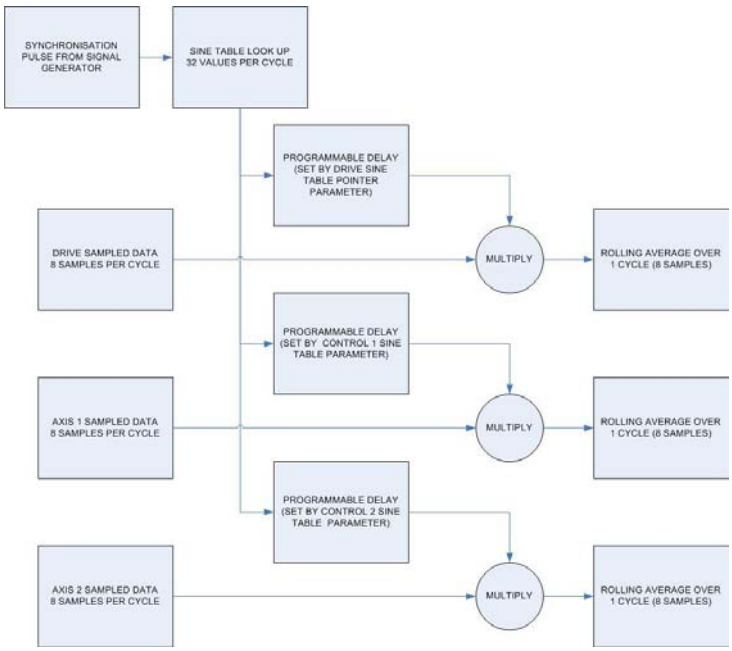

Figure 4 - Control FPGA computations

Figure 4 shows the computations implemented in the control FPGA, The offset into the sine table associated with each signal is controlled by a parameter which can run from 0 to 31, allowing phase adjustments with a resolution of 11.25 degrees (the parameters can be set through the web server interface of the Active Magnetic Bearing (AMB) controller and so can be set remotely if required). The resulting reference value is then multiplied by the associated sample value. The output of the multiplier is then processed as a rolling mean average across the preceding 8 samples (1 cycle). The FPGA is well suited to this sort of high speed (relatively simple) computation.

The rolling average computation, has a well defined phase characteristic (even when operating in the sampled system) and has the potential to provide a higher sensor bandwidth than the conventional low pass filter used with analogue signal conditioning. However, no investigation into comparative sensor bandwidths was conducted in this study (although some of the noise measurements reported later in this paper are consistent with this expectation). The rolling averages which represent the amplitude of the in-phase components of the waveforms are passed to the DSP which then performs the ratio-metric (division) function and the other computations shown in Figure 5. The use of the ratio-metric function ensures that any variation in the amplitude of the drive waveform (due to thermal effects, load variations due to impedance change etc) is eliminated. Additional functions performed by the DSP on these signals include filtering the drive waveform to eliminate any high frequency noise and calibration of the resulting signal to give a value in "engineering units" which can be used by the controller for the various computations for which position is required. This includes: position servo control; position alarms/trips; position summary values (peak and average) for transmission to trend monitoring or data acquisition systems; Trip data (a high speed capture buffer), Signal processing functions which allow for computation of Transfer Functions, Spectra or Order Tracked data.

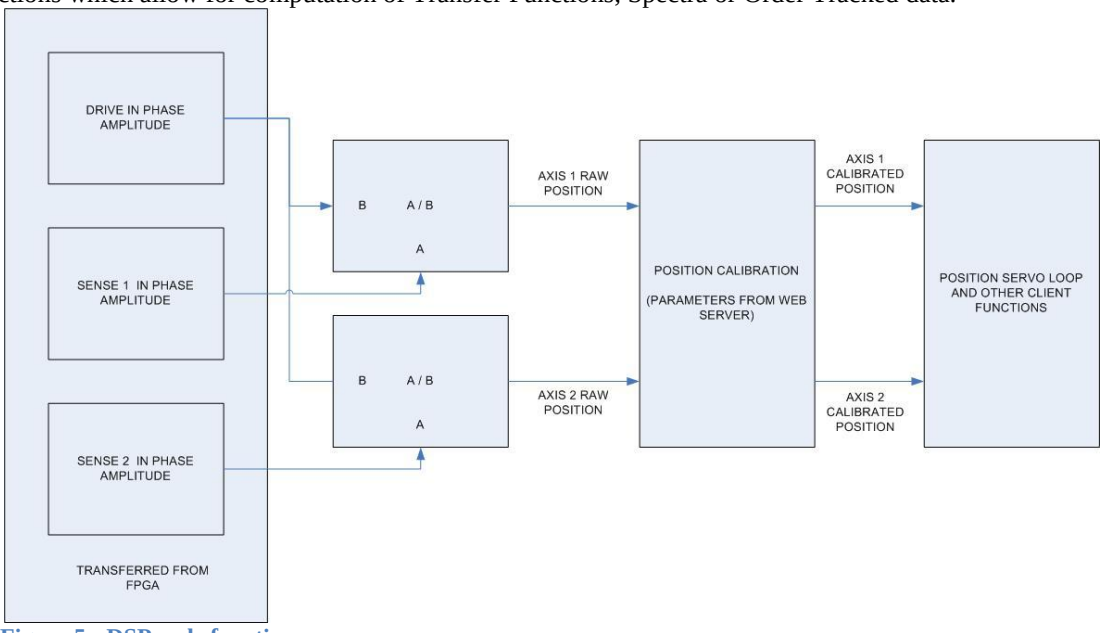

Figure 5 - DSP code function

In order to set up the phasing, it is necessary to offset the rotor from its centre position so that the inductive bridge is unbalanced. Once this position is established then a search is performed for the correct phase setting by looking for the maximum magnitude of the demodulated signal when plotted against the phase parameter. Alternatively the search can be for where the sign of the de-modulated signal crosses through zero, and then adjusting the phase parameter by 90 degrees. It is preferred to

offset the position so that the inductive bridge is un-balanced, otherwise it can be difficult to accurately set the phase reference, and particularly if the bridge is well balanced at the centre position and the resulting sensor output is zero. Such offsetting of positioning is not difficult and can be achieved by driving current into specific quadrants of the AMB to pull the rotor to a specific position within the auxiliary bearing clearance. When conducting commissioning at the end user site, this set up should be done with the final field cables in place. However, the final field cables are not always available for the OEM commissioning and so there may be a different set up during OEM commissioning, but since this is a simple parameter adjustment (rather than a component change requiring the use of a soldering iron) it is easily performed.

3 Test Methods

Tests were conducted on two types of test machine. The first were two 1.45MW motor driven hydrogen compressors in which both the motor and compressor were levitated with their own Zephyr controller (The controller from Waukesha for lower power equipment). This controller has the novel sensor demodulation circuit integrated. In this paper we present the results from the motors only.

The second tests were conducted using a small high speed test rig at the Waukesha Worthing facility (see Figure 6). This was used for comparative testing of conventional signal conditioning compared with the novel signal conditioning circuit.

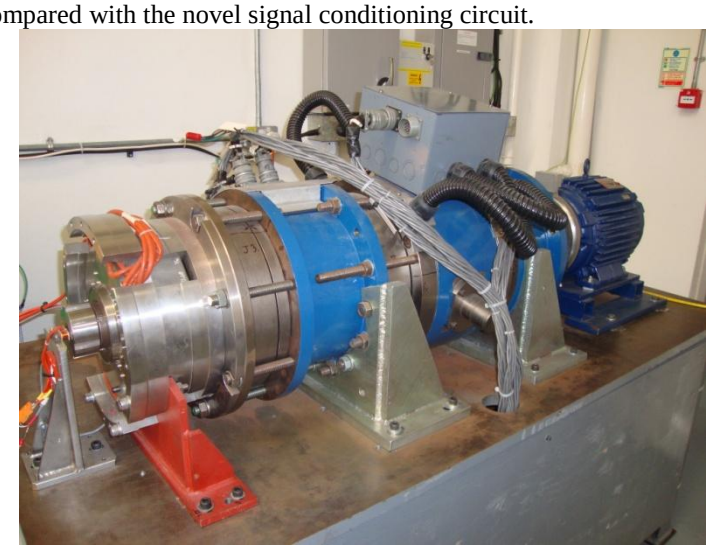

Figure 6 - Worthing Small Test Rig

3.1 Motor-Compressor

The Motor-Compressor is a 1.45MW unit which has a maximum speed during normal operation of 10,500 rpm and a maximum speed during factory testing of 11,500 rpm. The Compressor rotor weighs 790 Kg, the Motor Rotor weighs 723 Kg and the total string length is 5.5m.

Following the tuning of the machine (and just prior to the acceptance test) the diagnostic analogue outputs from the AMB controller were used together with an external dynamic signal analyser to record the spectrum of the position signals when in the de-levitated and levitated states. The peak amplitudes reported on the web-server interface of the AMB controller were also recorded.

3.2 Worthing Test Rig

The Worthing test rig has a 80 Kg rotor which has configurable dynamics and runs to a maximum speed of 12,000 rpm.

Figure 7 - Zephyr Controller (The control card of figure 3 is inside this unit)

This rig is normally equipped with a standard Waukesha Zephyr AMB controller (see Figure 7), but for the purposes of comparative testing, the test the rig was also tested with a Waukesha Chinook controller (see Figure 8) (The controller from Waukesha for medium power equipment). This was fitted with conventional inductive sensor signal conditioning.

Figure 8 - Chinook Controller

In both cases the diagnostic analogue outputs from the relevant AMB controller were used together with an external dynamic signal analyser to record the spectrum of the position signals when in the de-levitated state. The system structure and measurement configurations can be seen in Figure 9 and Figure 10). The peak amplitudes reported by the interface of the AMB controller were also recorded.

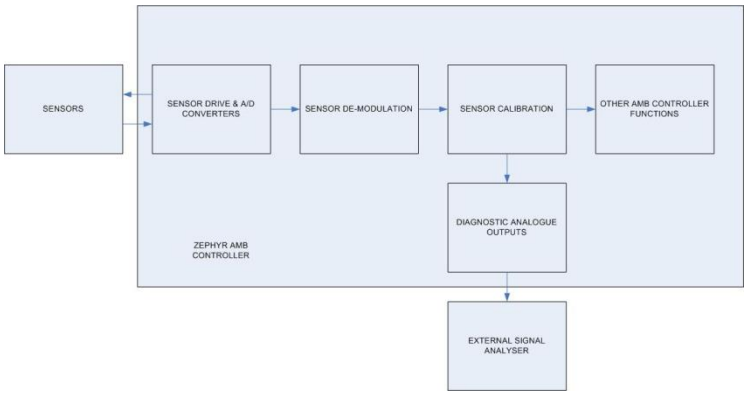

Figure 9 - Zephyr System Structure and measurement topology

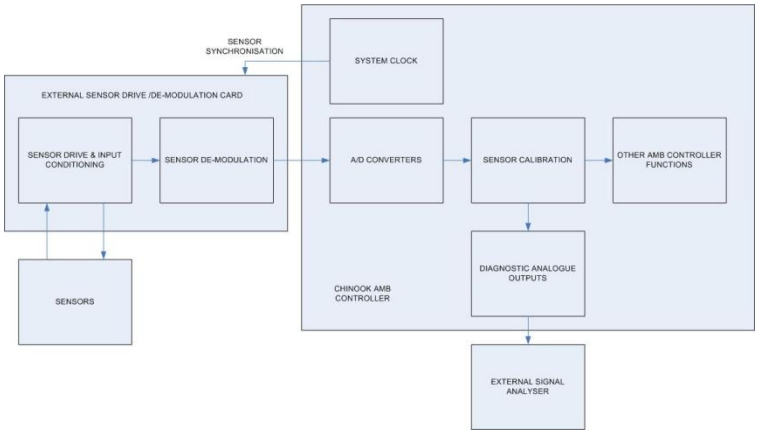

Figure 10 - Chinook System Structure and Measurement Topology

4 Test Results and Discussion

4.1 Motor/Compressor

A typical de-levitated position spectrum from one of the motor position signals is shown in Figure 11. The noise floor is at around 0.03 um (30nm), however there are distinct spectral lines, particularly at around 680Hz. The peak amplitude observed is 100nm and whilst we would look to reduce this, this is not a cause for concern (representing 0.05% of full scale). The peak amplitudes observed on the display of the AMB controller when de-levitated were 2um.

A typical levitated position spectrum from one of the motor position signals is shown in Figure 12. This shows a broadband noise floor at around 150nm with a low frequency peak of 2um at 18Hz. This response includes the effects of both position sensor noise and current sensor noise and the peak aligns with one of the rigid body modes of the motor. The peak amplitudes observed on the display of the AMB controller when levitated were 3um.

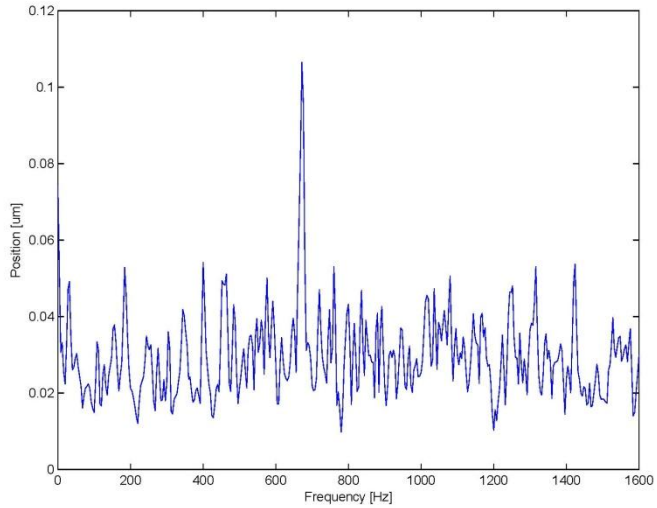

Figure 11 - Motor De-levitated Position FFT

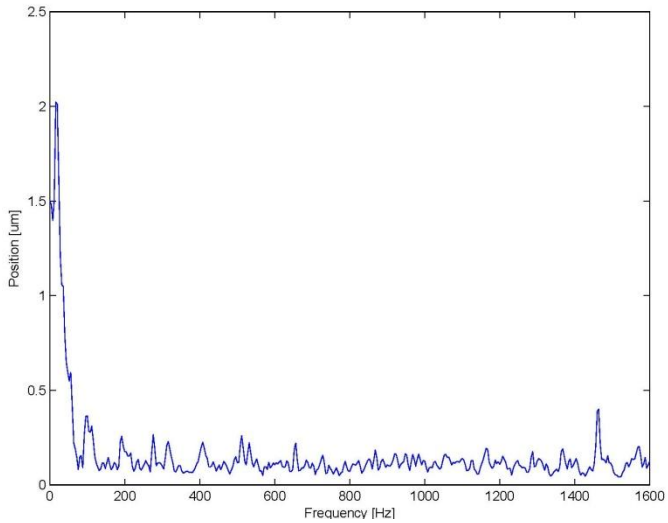

Figure 12 - Motor Levitated Position FFT

4.2 Worthing Test Rig

Figure 13 shows a comparison of typical FTT's of the de-levitated position signals for the conventional and the new design of sensor de-modulation.

The noise floor is broadly comparable at approximately 15nm in both cases. However, the conventional system shows a slightly higher noise level at low frequency and the new system shows a slightly higher noise level at high frequency (although this is entirely consistent with the wider bandwidth which is expected from the new de-modulation circuit).

Whilst both systems show spectral lines above the noise floor (particularly in the 600 to 1KHz region) it is noted that there appear to be slightly more lines associated with the novel sensor.

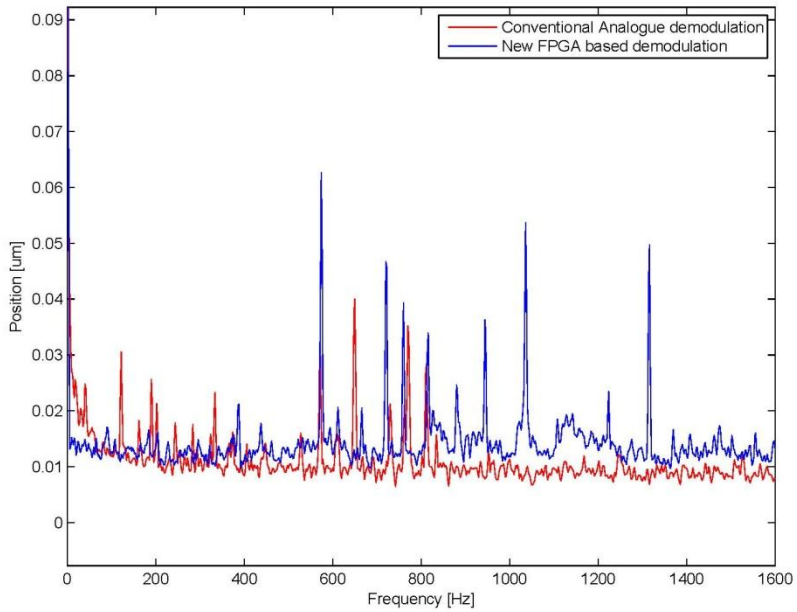

Figure 13 - Test Rig De-levitated Position FFT's for conventional and new de-modulation circuits

The matching of the controllers and the sensor calibration can be seen from the open loop transfer function measurements (see Figure 14) taken with each of the controllers in the levitated condition.

Table 1 shows the peak positions observed on the AMB controller display for both controllers in both the levitated and de-levitated conditions. The resolution of this display is limited to 1um and so it is not possible to make any significant observations on this data.

Table 1 - Peak Positions Observed on Controller Display

	Chinook (conventional)	Zephyr (Novel)
De-Levitated	1um	2um
Levitated	1um	1um

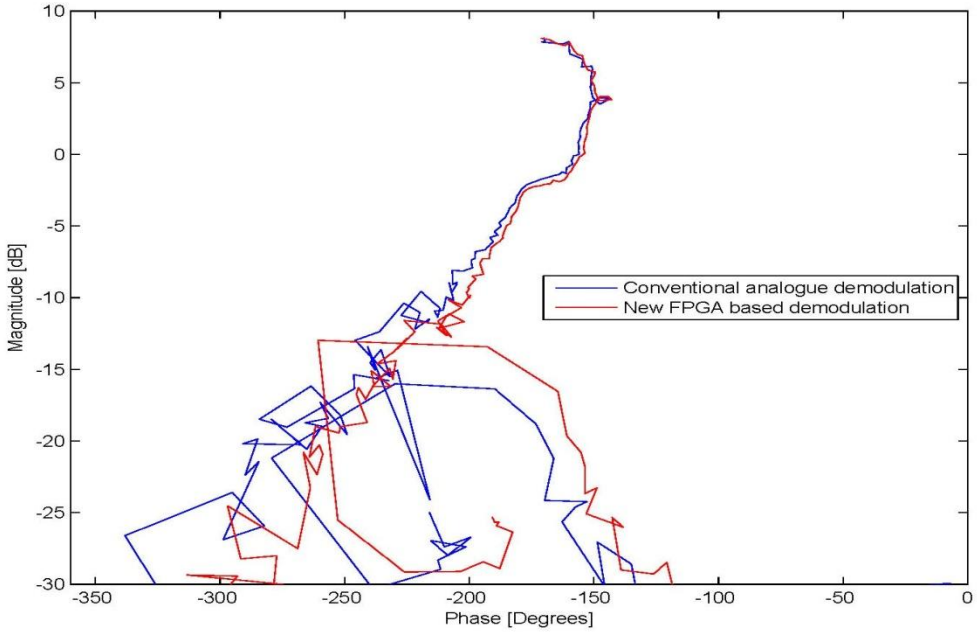

Figure 14 – Test Rig Nichols plots of OLTF for conventional and novel demodulation circuits

5 Conclusions and Further Work

Experimental measurements on a novel sensor demodulation circuit show comparable performance to existing analogue de-modulation circuits. Whilst there is some minor increase in the noise levels, the benefits of reduced cost and ease of set-up outweigh this.

Further investigation to identify (and eliminate) the source of the spectral lines observed in the measurements is planned.

Additional work on characterizing the noise levels observed in the compressors will be undertaken during end-user commissioning of the motor-compressor units. This is particularly of importance for the axial sensor, which uses a slip sensor type arrangement.

Additionally, the latest version of the Zephyr controller has a number of improvements over the system described here:

a) The maximum sample rate of the ADC has been increased allowing either larger numbers of samples to be captured per cycle of the sensor carrier frequency or a higher sensor carrier frequency to be used (as would be used for a bridge type eddy current sensor).

b) The 4 separate FPGA chips have been condensed into a single large FPGA, reducing transport delays between the separate chips.

The major outstanding work associated with this is to characterize the impact of these changes on the results presented here.

References

Burdett, R. (2005). Amplitude Modulated Signals: The Lock-in Amplifier. In P. Sydenham, & R. Thorn, *Handbook of Measuring System Design* (pp. 1197-1207). John Wiley and Sons Ltd.

Dam, B., Banerjee, K., Majumdar, K., Banerjee, R., & Patranabis, D. (2005). A Zero phase-lag homodyne demodulation technique for synchronous measurement applications and its FPGA implementation. *Journal of Circuits, Systems and Computers* , 771-791.

Rahal, M., & Demosthenous, A. (2009). An integrated signal conditioner for high-frequency inductive position sensor. *Measurement Science and Technology* .

Traxler, A., & Maslen, E. (2009). Hardware Components. In G. Schweitzer, & E. Maslen, *Magnetic Bearings* (pp. 101-102). Zurich: Springer.

Wu, S.-T., & Hong, J.-L. (2010). Five point amplitude estimation of Sinusoidal Signals: with application to LVDT Signal Conditioning. *IEEE Transactions on Instrumentation and Measurement* , 623-630.